Rigorous Evaluation of the Vertex Effects on the Frequency-Dependent Circuit Parameters of an Open-Ended Microstrip Line

Sandrino Marchetti, *Member, IEEE*

***Abstract*—This study presents the original inclusion of right singular vertex conditions in integral equations solved by the method of moments for accurate evaluation of frequency-dependent microstrip discontinuity models required in microwave integrated circuits (MIC) and monolithic microwave integrated circuits (MMIC) design. The 90° wedges singularity function for the current density, weighted with a novel sampling function for "corner cells," and the harmonic Green's function for shielded structures, is accurately and efficiently integrated in the conical geometry of the 90° sector. The frequency-dependent effective length and excess equivalent capacitance of a shielded open-ended microstrip line are calculated to a higher accuracy with respect to previous two-dimensional and three-dimensional "full wave analyses."**

***Index Terms*—Microstrip transmission line, printed antennas.**

I. Introduction

PRACTICALLY all printed circuits and antennas for microwave and millimeter wave applications make use of very thin conductors of polygonal contour presenting some sharp wedges, where the electromagnetic (EM) fields may assume singular vertex behaviors [16]. Nowadays more accurate "full wave analyses" for passive circuit components like transformers, filters, mixers, resonators, antennas, etc., still do not include these singular conditions. This is probably due to the fact that the simpler formulation of proper weighting functions has been presented only recently [2], [3] and still their introduction in the named algorithms does not appear to be obvious. From a very large number of previous studies dealing with such discontinuities, summarized in books like [1], [14], [15], the inaccuracy in determining some equivalent circuit elements has been often attributed to problems of convergence for the set of functions used to describe approximately the vertex effects. However, more accuracy for the EM simulation of such singular behavior is increasingly important at higher microwave and millimeter-wave frequencies where, in addition, de-embedding of the measurements and repeatability of the same are difficult. Moreover, in dealing with monolithic microwave integrated circuits (MMIC's), the CAD software should account also for the possible interactions among elementary discontinuities since they operate in the same electromagnetic environment.

Manuscript received July 5, 1996; revised February 2, 2000.

The author is with the Université de Nice-Sophia Antipolis, CNRS-Bat. 4-S.P.I., 06560 Valbonne, France.

Publisher Item Identifier S 0018-926X(00)04368-4.

In this context, we start (as a way of example) by developing a rigorous analysis for the classic problem of the open-end microstrip line, which, for its circuit versatility, has been object of an incredibly large number of investigations and applications (see among the others works [4]–[8], [10], [12]). From previous works the termination has been found electrically equivalent to an excess frequency-dependent capacitance, strongly influenced by the dielectric substrate thickness and permittivity and by all of the near by conductors. From the point of view of [2] and [3], the abrupt end is equivalent to two contiguous wedges of 90° angular aperture where the charge and current densities assume a well-quantified singular behavior associated with a lumped capacitance and inductance, respectively.

Our original contribution, in this paper, consists in the inclusion of the vertex conditions in a relevant electric field integral equation (EFIE) solved by the method of moments (MoM). From the recovered distribution of current, the effective length and equivalent excess capacitance are evaluated. The reliability of this approach is based on the development of an original mathematical apparatus in conical geometry. It performs the analytical integration of the 90° sector current singularity weighted with a novel sampling function and the appropriate harmonic Green's function. This mathematical tool is assisted by a very efficient curve-fitting program which recovers the propagation constant and the reflection coefficient of the open end from current evaluations. Comparison with previous analyses, results, and measurements confirms that inclusion of the correct vertex conditions is the dominant factor in obtaining accurate effective length evaluations with respect to any sampling of the longitudinal current on the strip or to any set of functions representing inaccurately the current density singularity at the vertices.

II. Theoretical Development

A. Definition of the Problem

The theoretical formulation makes reference to the shielded open-end microstrip line printed on RT-duroid™ and presenting the geometrical dimensions drawn in Fig. 1. Throughout the work we always assume sinusoidal excitation (that where not otherwise specified) is the center frequency of the Ku-band (15 GHz) where the line exhibits a characteristic impedance $Z_0 = 50\ \Omega$. Other simplifications, for the purpose of this study, are that the strip is thin and perfectly conducting and its width

is small compared to the microstrip wavelength ($2b = 0.75$ mm $\ll \lambda_g = 14.5$ mm). Consequently, the strip transverse current density J_x is different from zero only at the vicinity of the discontinuity and the longitudinal current density distribution J_z follows the laws for uniform lines away from discontinuities.

The method determines J_z and the open-end excess capacitance by using an EFIE that is solved by the MoM using Galerkin's technique. Hereafter, for reasons of brevity, we focus the attention to the advantages of including vertex conditions in the framework of the complete formulation reported in [10]. Making use of the continuity equation, the integral equation that expresses the E_z component of the electric field at the air-dielectric interface $y = h$ is

$$E_z(x,h,z) = \int_{S\ \mathrm{strip}} G_{zz}(x,h,z;x',h,z')J_z(x',z')\,dx'\,dz' \tag{1}$$

where G_{zz} is the appropriate component of the electric dyadic Green's function as given in [9], [10] and S_{strip} is the surface of the strip conductor.

B. Definition of the Cells of Current

In solving (1) by MoM, the unknown J_z is expressed as a series of orthonormal test functions, each different from zero only in a section of the strip, namely the elementary current cell (see Fig. 2). By a preliminary implementation of an auxiliary mixed potential integral equation not accounting for singularities, it has been possible to reveal the type and position of the excited singularities (see [16]). The obtained current distribution is schematically depicted in Fig. 3 and shows that a distributed singularity of current is present at any point of the strip edge except at the point D where a singularity of charge occurs (see [3, fig. 2]). The singularity of current is of degree $-1/2$ at any point of the straight edge but $-0.185\,345$ at the 90° tip A, whereas the singularity of charge in D exhibits $-1/2$ strength. The geometry of the cells and the shape of the test functions can be chosen with some arbitrariness, but the efficiency of the algorithm and the accuracy of the solution are strongly enhanced if they contain *a priori* the correct known singular behavior of the current at the conductor edge. To this end we define a variety of cells, namely generator cell, body cells, corner cells, and open-end cell schematically depicted in Fig. 2. On each cell a local coordinate system X_i, Z_i is fixed except for the corner cells where the X, Z coordinates are used. Specifically, for the evaluation of the reflection coefficient, the line can be excited by an ideal gap generator localized at the first cell; that is, the generator cell [12]. The central part of the strip is subdivided into body cells, as wide as the strip and at which edges the current exhibits singular straight edge behaviors. The wedges of 90° angular aperture are fitted by corner cells where the current exhibits singular vertex behavior. The maximum radius of influence $r_{\max}$ of the 90° wedge singularity can be evaluated as (see [2], [3]):

$$\kappa r_{\max} = \frac{1}{N_d} \tag{2}$$

where κ is the free-space wavenumber at 15 GHz and N_d is typically between 10 and 100. Since the width of the strip is

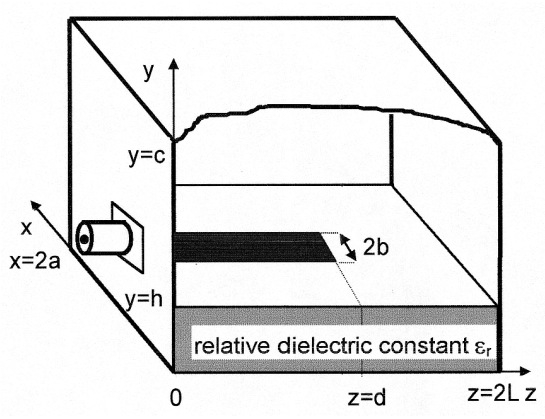

Fig. 1. Shielded open-ended microstrip line exited by a coaxial cable: $2a = 7.11$ mm, $c = 3.56$ mm, $2L = 32.7$ mm, $d = 18$ mm, $2b = 0.75$ mm, $h = 0.254$ mm, $\epsilon_r = 2.22$.

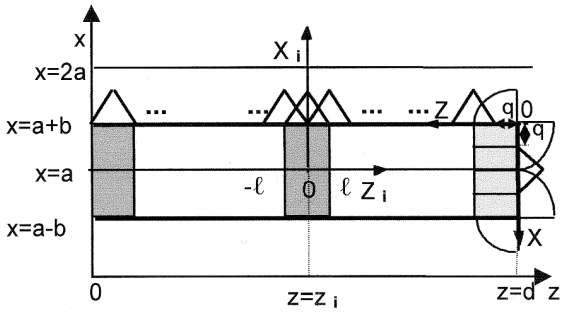

Fig. 2. Strip subdivision in current cells with relative local coordinate systems and sampling functions.

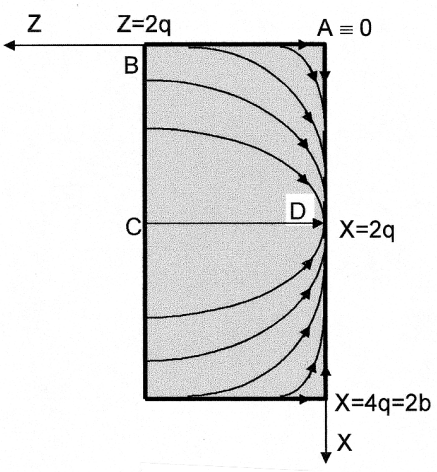

Fig. 3. Lines of current at the open-end and corner cells.

0.75 mm, we do not commit appreciable error considering the influence of the vertex singularity extended just up to the center of the strip, i.e., choosing $r_{\max} = 2q = 0.75/2 = 0.375$ mm. In addition, if we choose for the corner cell the square form depicted in Fig. 3, the symmetry with respect to the bisecting line AC of the fundamental H-mode current density (see [3, fig. 2a]), permits one to recover the principal part of J_x simply by using

$$J_x(X,Z) = -J_z(Z,X). \tag{3}$$

Finally, an open-end cell is to be considered at the center of the strip termination, half overlapping each corner cell and at which conductor edge J_z vanishes with a zero of degree 1/2. Imposition of the latter condition together with the vanishing of J_x in $x = a$ ensures the behavior of the main current and singular charge characteristics associated with the fundamental E-mode relative to the point D in Fig. 3 (see [3, fig. 2b]).

C. The Choice of the Test Functions

The Green's function in (1) can be put in the following form [9], [10]:

$$G_{zz}(x,h,z;x',h,z') = \sum_{N=1}^{\infty}\sum_{M=0}^{\infty} f(\kappa,k_x,k_z)\sin(k_x x)\cdot\sin(k_x x')\cos(k_z z)\cos(k_z z') \tag{4}$$

where $k_x = N\pi/2a$ and $k_z = M\pi/2L$ are the discrete wavenumbers along x and z, respectively, while $f(\kappa,k_x,k_z)$ is a function of the geometry, frequency and dielectric permittivity as well as of the wavenumbers; its explicit expression can be found in [9], [10]. The solution of (1) by the MoM using Galerkin's technique, requires the evaluation of the following coefficients:

$$C_{i,M,N} = C_i(k_x,k_z) = \int_{\text{cell } i} \sin(k_x x')\cos(k_z z')\cdot J_i(x',z')\,dx'\,dz' \tag{5}$$

for all cells of the strip.

In (5) $J_i(x',z')$ is the test function for cell i, which we express for convenience as the product of an amplitude I_i, a weighting function $w_i(x',z')$, and a sampling function $j_i(x',z')$. The weighting function contains the known singular conditions specified in the previous subsection, whereas the simple sampling function is chosen to provide at once analyticity and fast convergence with respect to k_x and k_z of the coefficients in (5). In the following equations, the geometry of the single cells are those shown in Fig. 2 which also shows schematically the sampling functions. For comparison purposes, we also include in this work a one-dimensional (1-D) analysis, where no singularities are considered and the test functions are reduced to the following triangular sampling functions:

$$J_i(x',z') = I_i w_i(x',z') j_i(x',z') = I_i \begin{cases} \left(1+\dfrac{Z_i}{\ell}\right), & -\ell \le Z_i < 0 \\ \left(1+\dfrac{Z_i}{\ell}\right), & \ell \ge Z_i \ge 0. \end{cases} \tag{6}$$

In (6) I_i is the unknown amplitude of the current at the center of the cell i.

When a two-dimensional (2-D) analysis is performed, the test function includes the straight edge singularity and can be formulated as follows:

$$J_i(x',z') = I_i \frac{1}{\sqrt{1-\left(\dfrac{X_i}{b}\right)^2}} \cdot \begin{cases} \left(1+\dfrac{Z_i}{\ell}\right), & -\ell \le Z_i < 0 \\ \left(1-\dfrac{Z_i}{\ell}\right), & \ell \ge Z_i \ge 0. \end{cases} \tag{7}$$

In the three-dimensional (3-D) treatment, (7) holds for the body cells, whereas for the corner cells the test functions must fit the vertex conditions as follows:

$$J_i(x',z') = I_i \frac{2^{(\nu+1)/2}}{q^{\nu-1}} \cdot \begin{cases} \dfrac{r^\nu}{\sqrt{2XZ}}\left(1-\dfrac{Z}{2q}\right), & 0 \le X < Z \le 2q \\ \sqrt{2XZ}\,r^{\nu-2}\left(1-\dfrac{X}{2q}\right), & 2q \ge X \ge Z \ge 0 \end{cases} \tag{8}$$

$r = \sqrt{X^2+Z^2}$ is the radial distance from the tip A in Fig. 3 and $\nu = 0.814\,655$ (see $\nu - 1 = \alpha = -0.185\,344\,7$ in [3, table II]). The weighting function in (8) is found from [1, table 2] or [3, table III] and the sampling functions are chosen in such a way as to increase analyticity in computing the coefficients (5), as shown in the next section. Finally, a test function satisfying a zero of degree 1/2 at the edge of the conductor in the open-end cell is given by

$$J_i(x',z') = I_i \sqrt{1-\left(\frac{Z_i}{q}\right)^2} \cdot \begin{cases} \left(1+\dfrac{X_i}{q}\right), & -q \le X_i < 0 \\ \left(1-\dfrac{X_i}{q}\right), & q \ge X_i \ge 0. \end{cases} \tag{9}$$

We should like to stress that only because of the previous choices for cells geometry and test functions the simple integral (1), which considers only the longitudinal current, takes into account *a priori* all the correct main current behaviors at the open-end. In fact, in spite of all previous test functions are for current in the z direction, the x-directed current at the open-end is forced by (3).

III. Integration of Vertex Singularities

The determination of the coefficients in (5) using the test functions given in (6), (7), and (9) is nowadays a common practice, hence, only their analytical expressions are reported in Appendix A. The determination of the same coefficients using the test function in (8) requires the use of the conical geometry of

the 90° sector and is of vital importance in the present methodology. Thus, we report a detailed formulation, writing

$$C_i(k_x,k_z)=I_i\frac{2^{(\nu+1)/2}}{q^{\nu-1}}\,(I_{ABC}+I_{ACD}) \tag{10}$$

where

$$I_{ABC}=\int_{ABC}\sin(k_x x')\cos(k_z z')\frac{r^\nu}{\sqrt{2XZ}}\cdot\left(1-\frac{Z}{2q}\right)^\nu dx'\,dz' \tag{11}$$

$$I_{ACD}=\int_{ACD}\sin(k_x x')\cos(k_z z')\sqrt{2XZ}r^{\nu-2}\cdot\left(1-\frac{X}{2q}\right)^\nu dx'\,dz'. \tag{12}$$

Two rectangular coordinate systems are involved in (11), (12) but neither of them is suitable for analytic and/or accurate evaluation of the integrals because of the spherical singularity at the tip $r=X=Z=0$. To avoid this problem we have to express the integrand in the conical coordinate system r, θ, ϕ centered at A and oriented with the equicoordinate surface $\theta=\pi$ fitting the corner cell [see [16, fig. 3] and Fig. 4(a)], i.e., satisfying the coordinates transformation

$$X=kr[\sqrt{1-(k\cos\phi)^2}-k\cos\phi]\equiv r\Phi_x(\phi) \tag{13}$$

$$Z=kr[\sqrt{1-(k\cos\phi)^2}+k\cos\phi]\equiv r\Phi_z(\phi) \tag{14}$$

where $k=1/\sqrt{2}$ is the parameter of this geometry and Φ_x, Φ_z are auxiliary functions of ϕ only. The elementary area is found to be transformed as follows:

$$dx'\,dz'=dX\,dZ=r\frac{\sqrt{\Phi_x\Phi_z}}{\Phi_x+\Phi_z}dr\,d\phi \tag{15}$$

and consequently the cell $ABCD$ is transformed as drawn in Fig. 4(b). In order to show the procedure, only the integration in the half cell ABC will be shown explicitly, starting by expressing the integrand in conical coordinates as follows:

$$I_{ABC}=\int_0^{\pi/2}\frac{1}{\Phi_x+\Phi_z}\int_0^{2q/\Phi_2}\sin[k_x(a+b-r\Phi_x)]\cdot\cos[k_z(d-r\Phi_z)]\left(1-\frac{r\Phi_z}{2q}\right)^\nu\cdot kr^\nu\,dr\,d\phi. \tag{16}$$

The singularity at the tip $r=0$ is no longer present, hence, numerical integration versus r of (16) may be performed accurately but requires long computation time in view of the fact the coefficients (5) are needed for a large number of k_x and k_z. The

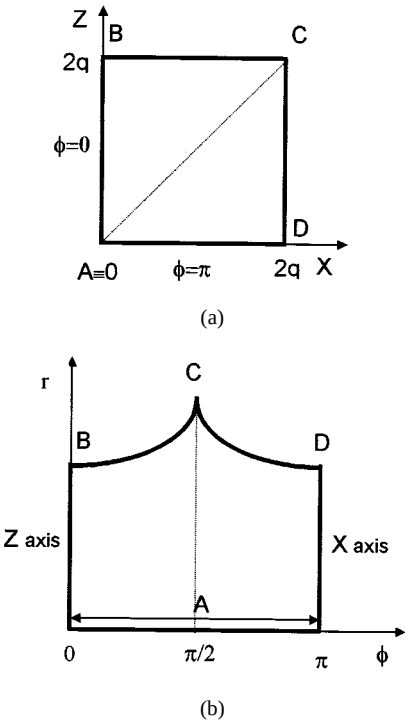

Fig. 4. Corner cell in (a) rectangular X-Z and (b) conical $r-\phi$ coordinates.

particular choice of the sampling function in (8) permits analytical integration along r (see [11, pp. 424–425]) reducing the integral (16) to

$$I_{ABC}=S\int_0^{\pi/2}\frac{1}{\Phi_z^{\nu+1}(\Phi_z+\Phi_x)}\cdot\left[\sin(C^+-z^+)\,\frac{J_{\nu+1/2}(z^+)}{z^{+(\nu+1/2)}}+\sin(C^--z^-)\,\frac{J_{\nu+1/2}(z^-)}{z^{-(\nu+1/2)}}\right]d\phi \tag{17}$$

where $S=\sqrt{\pi}\Gamma(\nu+1)/2q^{(\nu+1)}$, $J_{\nu+1/2}$ is a Bessel function of the first kind of order $\nu+1/2$ and

$$C^\pm=k_x(a+b)\pm k_z d,\qquad z^\pm=q\left(k_x\frac{\Phi_x}{\Phi_z}\pm k_z\right). \tag{18}$$

Also the integration along ϕ becomes analytically possible if the integrand functions in (17) are expanded in a double series using the Graf's addition theorem and the series representation of the product of two Bessel functions as follows [13]:

$$\begin{aligned}&\sin(C^+-z^+)\,\frac{J_{\nu+1/2}(z^+)}{z^{+(\nu+1/2)}}+\sin(C^--z^-)\,\frac{J_{\nu+1/2}(z^-)}{z^{-(\nu+1/2)}}\\&=\sum_{n=0}^{\infty}A_n\frac{J_{n+\nu+1/2}(qk_z)}{(qk_z)^{(\nu+1/2)}}\sum_{m=0}^{\infty}\cdot\left[a_n(k_x,k_z)+b_n(k_x,k_z)qk_x\frac{\Phi_x}{\Phi_z}\right]\cdot B_{nm}\left(qk_x\frac{\Phi_x}{\Phi_z}\right)^{n+2m}\end{aligned} \tag{19}$$

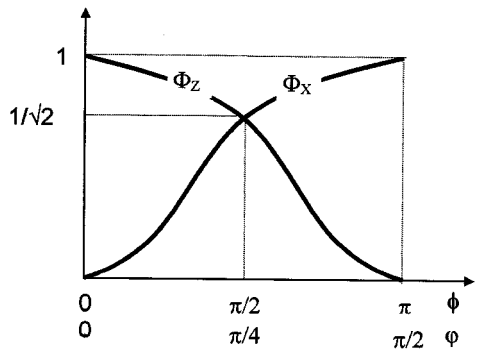

Fig. 5. Auxiliary functions Φ_x and Φ_z versus the conical coordinate ϕ and the auxiliary variable φ.

where A_n, B_{nm}, a_n, b_n are specified in Appendix B. In this way the integration versus ϕ is reduced to evaluate the elementary integrals of general form

$$I_j = \int_0^{\pi/2} \frac{1}{\Phi_z^{\nu+1}(\Phi_x + \Phi_z)} \left(\frac{\Phi_x}{\Phi_z}\right)^j d\phi \quad \text{for } j = 0, 1, 2, \cdots. \tag{20}$$

Further, noting that the auxiliary functions Φ_x, Φ_z formulated in (13) and (14) satisfy to the properties

$$\Phi_x^2 + \Phi_z^2 = 1, \quad \Phi_z - \Phi_x = \cos\phi, \quad \Phi_x \Phi_z = (k \sin\varphi)^2 \tag{21}$$

it is possible to change ϕ with an auxiliary variable φ according to the following transformation (see Fig. 5)

$$\phi \in [0, \pi], \quad \Phi_x = \sin\varphi, \quad \Phi_z = \cos\varphi, \quad \varphi \in \left[0, \frac{\pi}{2}\right]. \tag{22}$$

Consequently, the integral (20) is reduced to the more familiar form

$$I_j = \frac{1}{\sqrt{2}} \int_0^{\pi/4} \left(\frac{\sin\varphi}{\cos\varphi}\right)^{j-1/2} \frac{1}{(\cos\varphi)^{\nu+2}} d\varphi \quad \text{for } j = 0, 1, 2, \cdots \tag{23}$$

which, using reduction formulas (see for example [11, p. 130]), can be expressed versus I_0 only

$$I_j = I_j(j, I_0), \quad \text{where} \quad I_0 = \int_0^{\pi/4} \frac{1}{\sin\varphi(\cos\varphi)^{\nu+1}} d\varphi. \tag{24}$$

Then we recover the following closed form:

$$I_{ABC} = S \sum_{n=0}^{\infty} A_n \frac{J_{n+\nu+1/2}(qk_z)}{(qk_z)^{\nu+1/2}} \sum_{m=0}^{\infty} B_{nm} \cdot [a_n(k_x, k_z) I_{n+2m} + b_n(k_x, k_z) I_{n+2m+1}]. \tag{25}$$

The integration of IACD given in (12) follows the previous lines and terminates with a form similar to (25). Hence, I_0 and another integral arising from the integration of I_{ACD}, are the sole forms to be integrated numerically by a NAG library subroutine and for this the coefficients $C_i(k_x, k_z)$ are said to be obtainable in a quasi-analytic way. In addition, taking into account the expressions of $a_n(k_x, k_z), b_n(k_x, k_z)$ reported in Appendix B, we can rearrange expression (25) in such a way the summation in m depends on k_x, but not on k_z. Computationally, this permits one to generate a quasi-recursive property of the form (25) that together with fast convergence properties of B_{nm} with m, n and of $J_{n+\nu+1/2}$ with n allows computation of a coefficients matrix $C_i(k_x, k_z)$ of dimensions $N_{\mathrm{stop}} \times M_{\mathrm{stop}} = 200 \times 1000$ in few minutes with an IBM RISC 6000/550. The observed accuracy is within a few % for the more critical large values of k_x, k_z when compared with the numerical integration of (16).

For symmetry reasons, the coefficients in the lower 90° corner cell are obtainable from the previous $C_i(k_x, k_z)$ simply by changing the sign when N is even and using the same value when N is odd.

IV. Obtained Results

The satisfaction of the boundary conditions $E_z = 0$ at the strip conductor, imposed in (1) using the MoM with Galerkin's technique, gives the following matrix equation:

$$[Z] \cdot [I] = [V] \tag{26}$$

where $[I]$ is the unknown vector of the current density amplitudes I_i at the center points of the N_c cells and $[V]$ is the excitation vector that for the present gap generator excitation method, presents only one nonzero value at the generator cell [12]. In (26) $[Z]$ is the $N_c \times N_c$ matrix of moments of elements Z_{ij} obtained using the coefficients (5) as follows:

$$Z_{ij} = \sum_{N=1}^{\infty} \sum_{M=0}^{\infty} f(\kappa, k_x, k_z) C_i(k_x, k_z) C_j(k_x, k_z) \cong \sum_{N=1}^{N_{\mathrm{stop}}} \sum_{M=0}^{M_{\mathrm{stop}}} f(\kappa, k_x, k_z) C_i(k_x, k_z) C_j(k_x, k_z) \quad \text{for } i, j = 1, 2, \cdots, N_c. \tag{27}$$

In order to avoid convergence problems we have chosen the maximum summation indexes $N_{\mathrm{stop}} \times M_{\mathrm{stop}} = 200 \times 1000$; the higher value of M_{stop} is due to the fact the function f varies as a constant and a constant times k_z when k_x and k_z go to infinity respectively [9]. Then a value of $d = 18$ mm is chosen for the strip length, corresponding to about 70 cells/wavelength. Furthermore, in order to facilitate the comparison of the solution [I] for 1-D, 2-D, and 3-D analyses, we choose $2\ell = 2q = b$ in Fig. 2, that is to say the union of the two corner cells reproduces a usual body cell when no vertex conditions are considered. Consequently, the $[Z]$ matrix is symmetric for the 1-D and 2-D cases, while for the 3-D case the symmetry fails only in the last three columns and rows associated with the two corner cells and with the open-end cell. Nevertheless, in all cases it is noted that the diagonal elements of $[Z]$ are dominant and the other elements taper off uniformly as one moves away from the diagonal, confirming a property common to all closed structures [10]. All

these properties are used to considerably reduce the computer time in determining $[Z]$ and in recovering the vector solution solving (26) as follows:

$$[I] = [Z]^{-1} \cdot [V]. \tag{28}$$

The propagation constant β and the open circuit reflection coefficient Γ_{oc}, through its amplitude ρ and phase γ, are used to compare the results of the three analyses and to simulate the electric behavior of the discontinuity. A negative value of γ indicates that the electric open circuit section is moved from the open-end by an effective length $L_{\text{eff}} = -\gamma/2\beta$ (mm). For characterizing the abrupt end the parameter L_{eff}/h is more commonly used, while for simulation purposes the same phase delay indicated by γ is reproduced by an equivalent excess capacitance of value $C = \tan(\beta L_{\text{eff}})/\omega Z_0(F)$ [10]. Summarizing, the situation of the strip feed by a 50-Ω coaxial cable, its electric equivalent, and the simulation using an ideal gap generator excitation can be schematized as in Fig. 6(a)–(c) respectively. The recovered current amplitude distributions for the 1-D, 2-D, and 3-D cases at the median line of the strip are reported in Fig. 7. The open-end region is enlarged in the insert in order to better show the significant decreasing of the current obtained with the 3-D analysis. From the same distribution we back out simultaneously β, ρ, and γ using a very accurate curve fitting program that compares the numerical evaluations of $[I]$ with the theoretical distribution of current pertaining to an ideal uniform line and parametrized just by β, ρ, and γ. From the fitting are excluded the data too close to the generator and open-end cells, where higher order modes are excited. The parameters so recovered are shown in Table I.

The β value obtained using an accurate alternative spectral domain technique is about 433 and the value of ρ given by the theory for an open line is 1 (notice that for the chosen geometrical dimensions and working frequencies, radiation losses due to couplings with the box conductors are negligible). Thus, according to Table I the fitting program that was used recovers these values very accurately leading us to believe that the value of γ is also very reliable. Surprisingly, the results show that the inclusion of the straight edge singularity of the 2-D case does not improve substantially the accuracy of L_{eff} with respect to a 1-D case because it does not contain more accurate information about the open end. The fact that L_{eff}/h for the 1-D and 2-D analyses is about 1.9 times larger than the correct 3-D one, is in part due to a missing optimization process for the sampling function shape as proved necessary in [10].

The current density surface distribution on the strip is shown in Fig. 8. The transverse current density J_x is recovered by using (3) and its behavior is shown in Fig. 9. Note that from (8), (3) and Fig. 9 it appears that J_x, J_z are discontinuous at the 90° tips proceeding along the conductor edge. Physically speaking, the singular current density flows along the edge and bends 90° suddenly at the tips as schematized in Fig. 3. We finally remark that the determination of J_x, J_z with classic analyses, not accounting for (3), requires a $[Z]$ matrix four times larger.

TABLE I
COMPARISON OF 1-D, 2-D, AND 3-D LINE PARAMETERS

dim	β (rad/m)	ρ	γ (rad)	L_{eff} (mm)	L_{eff} / h
1D	432.7	1.00	-0.106	0.123	0.548
2D	433.2	1.00	-0.101	0.117	0.520
3D	432.8	1.00	-0.055	0.064	0.284

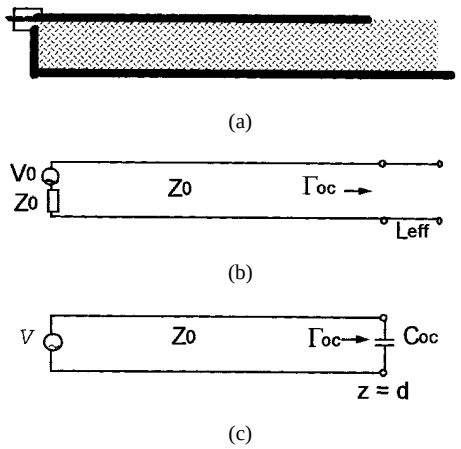

Fig. 6. Open-ended microstrip line excited by coaxial cable. (a) Physical line. (b) Equivalent electric line. (c) Ideal simulated line.

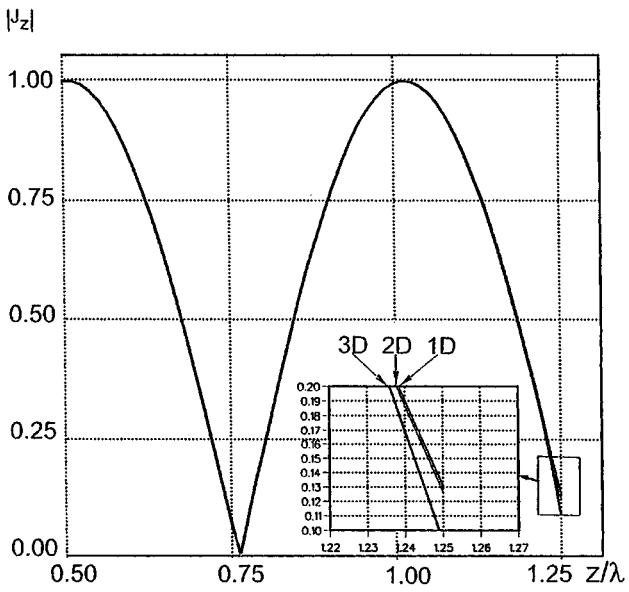

Fig. 7. Module of the density of current J_z at the microstrip median line relative to 1-D, 2-D, and 3-D analyses.

V. EFFECTIVE-LENGTH FREQUENCY DEPENDENCE

For the sake of comparison we implement our program for a microstrip printed on allumina substrate $(\epsilon_r = 9.6)$, with $Z_0 = 40\ \Omega$ at 15 GHz, as analyzed in [4], [7], [8]. We choose a length $d = 24.176$ mm and a cell subdivision of about 30 cells/wavelength. The recovered values of β and ρ agree when 1-D, 2-D, or 3-D analyses are performed when L_{eff}/h is equal to 0.72, 0.71, and 0.31, respectively. Only the last value is in excellent accordance with those reported in [7] and [8].

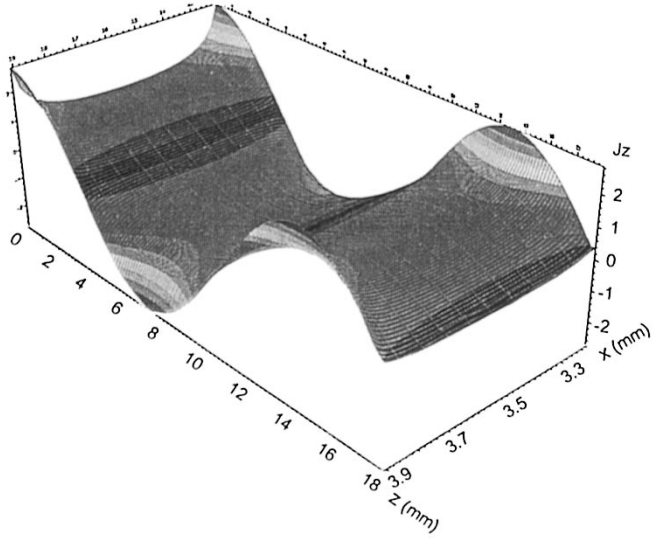

Fig. 8. Density of current J_z on the strip surface for a complete 3-D analysis.

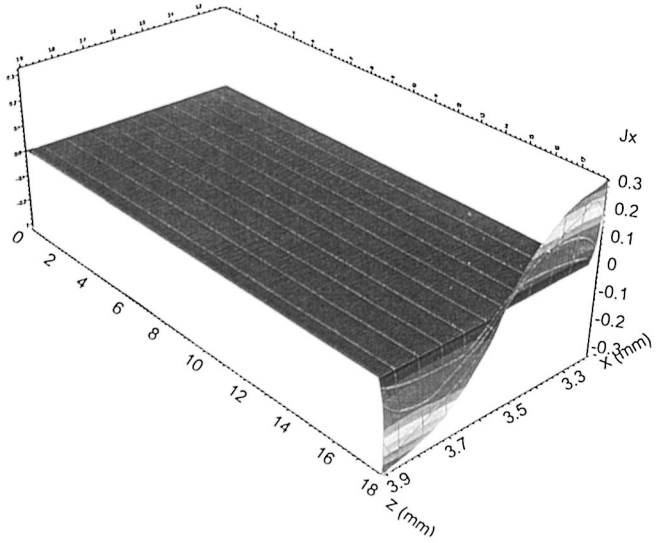

Fig. 9. Density of current J_x on the strip surface for a complete 3-D analysis.

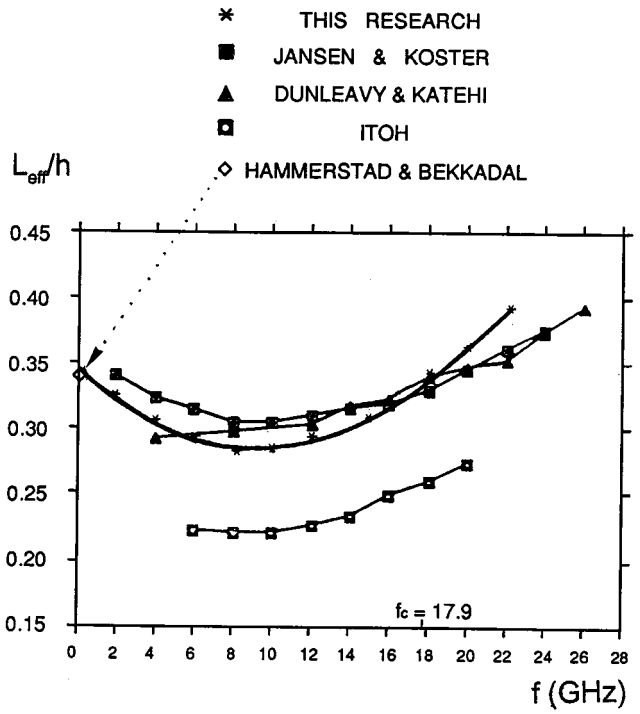

Fig. 10. L_{eff}/h relative to the open-ended microstrip line of parameters $2a = 7.747$ mm, $c = 5.08$ mm, $2L = 32.7$ mm, $d = 24.176$ mm, $2b/h = 1.57$, $h = 0.635$ mm, and $\epsilon_r = 9.6$.

For evaluating the frequency dependence of L_{eff}/h, we should remember that our modeling for the vertex singular conditions can be considered valid at most in the range [2, 20] GHz where condition (2) is satisfied assuming $r_{\max} = 2q \cong 0.5$ mm. Further, for this same gamma, the curve fitting program that evaluates β, ρ, and γ works correctly in spite of the fact that current distribution data are available only for a fraction of λ at the lower frequencies. The calculated values of L_{eff}/h are marked in Fig. 10. A static value of L_{eff}/h can be extrapolated from our curve in Fig. 10 by using simple interpolation of available data. This provides a static value close to the one obtained with a static analysis by Hammerstad and Bekkadal [5].

Concerning the frequency dependence, Fig. 10 shows that our data are in better agreement with those of the 3-D analysis reported in [7] where Jansen estimated an absolute error within 1% in the obtained values. The present analysis shows somewhere a discrepancy a little bit bigger than 1% that we believe is due to the spherical nature of the vertex singularity that is not considered in [7], where the current is represented by the product of a function solely of X and one solely of Z.

From the comparison with the 2-D analysis by Dunleavy we argue that better accuracy is due to the weighting functions at the open-end rather than to the optimization of the test functions shape and number for wavelength (respectively indicated with K and l_x in [8]) because we have used simple triangular functions and only 30 samples/wavelength.

Lastly we can add the following conclusions to those of Jansen [7], Itoh [4], and Dunleavy [10] about the two physical concurring phenomena responsible for the frequency dependence of L_{eff}/h. The open-end can be thought to be equivalent to a capacitive effect related to the deposition of charge by J_z and an inductive effect produced by the transverse current J_x. In the static case $J_x = 0$ and the open-end and the ground plane conductor constitute a pure capacitance. When the frequency increases, the inductive effect of the current J_x decreases the equivalent capacitance. For higher frequencies additive capacitive couplings (antenna effects) with conductors other than the ground plane should be accounted for. Of particular importance are the box resonances and the propagation of the second-order mode which has a cutoff frequency of $f_c = 17.9$ GHz. In order to validate these hypotheses, I have made some significant changes in the dimensions of the box and then the variations in L_{eff} at 4, 18, and 22 GHz were determined. Unfortunately, the actual measurement techniques for this accurate frequency dependence suffer from repeatability measurement errors (see [6], [8]).

$$A_{n+1} = \frac{(2n+2\nu+3)(2+2\nu+1)}{(2n+2\nu+1)(n+1)} A_n, \qquad A_0 = 1$$

$$B_{n,m+1} = -\frac{(n+\nu+2m+2)(n+\nu+2m+1)}{(m+1)(2m+1)(2n+2\nu+2m+3)} \cdot \frac{B_{n,m}}{(n+\nu+m+1)}$$

$$B_{n+1,0} = \frac{1}{2n+2\nu+3} B_{n,0}, \qquad B_{0,0} = 1$$

VI. Further Developments

The presented algorithm is suitable for investigating the behavior of L_{eff}/h versus strip and box dimensions as well as substrate thickness and dielectric constant as required in CAD for MIC's and MMIC's. However, further developments will be also addressed to accurately evaluate the frequency dependent lumped elements associated with other microstrip discontinuities including 270° and/or any aperture vertices. Mixed potential integral equations will be employed in the more general case where current and charge singularities are both excited and accounted for. The study can be extended to open circuits and antennas with obvious differences in the Green's functions and moment-method matrix.

VII. Conclusion

The effective-length frequency dependence of an open-ended shielded microstrip line has been originally evaluated by including the effects of the EM singularities at the open end. In solving the EFIE by the MoM, the singularities are accounted for by a novel choice of the current cells geometry and the associated test and weighting functions. The accurate evaluation of the matrix of moments has required the use of a suitable conical geometry for the 90° sector. The comparison with previous works shows that satisfying *a priori* the known vertex conditions is a dominant factor in obtaining efficiency and accuracy with respect to optimization and/or convergence problems of the functions approximating the current behavior at the open end. Consequently, this study constitutes a further refinement and a deeper insight into the physical phenomenon associated with the open-end microstrip line showing the role and quantitative effect of the EM singularities. It also constitutes the starting study for analyzing any printed circuit discontinuity with this methodology.

Appendix A

The coefficients in (5) relative to the body cells and generator cell are given by

$$C_i(k_x, k_z) = I_i 4\ell b \sin(k_x a) \cos(ik_z\ell) F_1(k_x b) F_2(k_z \ell)$$

where

$$F_1(k_x b) = \begin{cases} \sin(k_x b)/(k_x b), & \text{for 1-D} \\ \pi/2 J_0(k_x b), & \text{for 2-D} \end{cases}$$

$$F_2(k_z \ell) = \begin{cases} (1-\cos(k_z\ell))/(k_z\ell)^2, & \text{for } k_z \neq 0 \\ 1/2, & \text{for } k_z = 0 \end{cases}$$

while for the open-end cell they are expressible as follows:

$$C_i(k_x, k_z) = I_i 4q^2 \cos(k_x q) \cos(k_z(d-q)) \cdot \frac{\sin^2(k_x q)}{k_x q} F_3(k_z q)$$

where

$$F_3(k_z q) = \begin{cases} \pi J_1(k_z q)/(k_z q), & \text{for } k_z \neq 0 \\ \pi/2, & \text{for } k_z = 0 \end{cases}.$$

In the former equations J_0 and J_1 are the Bessel functions of order zero and one, respectively.

Appendix B

The coefficients A_n, B_{nm}, which appear in (19) can be expressed through their recursive formulas as shown at the top of the page, while the coefficients $a_n(k_x, k_z), b_n(k_x, k_z)$ are given by

$$a_n(k_x, k_z) = a_{n1}(k_x) a_{n2}(k_z)$$

where

$$a_{n1}(k_x) = \begin{cases} \sin(k_x(a+b)), & n \text{ even} \\ \cos(k_x(a+b)), & n \text{ odd} \end{cases}$$

$$a_{n2}(k_z) = \begin{cases} 2\cos(k_z(d-q)), & n \text{ even} \\ -2\sin(k_z(d-q)), & n \text{ odd} \end{cases}$$

and

$$b_n(k_x, k_z) = \frac{(n+2m+\nu+1)}{(2m+1)(n+m+\nu+1)} b_{n1}(k_x) b_{n2}(k_z)$$

where

$$b_{n1}(k_x) = \begin{cases} \sin(k_x(a+b)), & n \text{ odd} \\ \cos(k_x(a+b)), & n \text{ even} \end{cases}$$

$$b_{n2}(k_z) = \begin{cases} -2\sin(k_z(d-q)), & n \text{ odd} \\ -2\cos(k_z(d-q)), & n \text{ even} \end{cases}$$

respectively.

References

[1] T. Itoh, Ed., *Numerical Techniques for Microwave and Millimeter-Wave Passive Structures*. New York: Wiley, 1989.

[2] S. Marchetti and T. Rozzi, "Electric field singularities at sharp edges of planar conductors," *IEEE Trans. Antennas Propagat.*, vol. 39, pp. 1312–1320, Sept. 1991.

[3] ——, "**H**-field and **J**-current singularity at sharp edges in printed circuits," *IEEE Trans. Antennas Propagat.*, vol. 39, pp. 1321–1331, Sept. 1991.

[4] T. Itoh, "Analysis of microstrip resonators," *IEEE Trans. Microwave Theory Tech.*, vol. AP-22, pp. 946–952, Nov. 1974.

[5] E. Hammerstad and F. Bekkadal, *Microstrip Handbook*, Norway: Univ. Trondheim, 1975, sect. III, p. 25.

[6] C. Gupta, B. Easter, and H. Gopinath, "Some results on the end effect of microstriplines," *IEEE Trans. Microwave Theory Tech.*, vol. MTT-26, pp. 649–652, Sept. 1978.
[7] R. H. Jansen and N. H. L. Koster, "Accurate results on the effect of single and coupled microstrip lines for use in microwave circuit design," *Arch. Elek. Ubertragung*, vol. 34, pp. 453–459, 1980.
[8] L. P. Dunleavy and P. B. Katehi, "Shielding effects in microstrip discontinuities," *IEEE Trans. Microwave Theory Tech.*, vol. 36, pp. 1767–1774, Dec. 1988.
[9] H. A. Ghaly, J. Citerne, and V. Fouad Hanna, "Complete dyadic Green functions for three-dimensional non radiating discontinuity analysis," *Soc. Int. Symp. Antennas Propagat.*, pp. 874–877, June 1991.
[10] L. P. Dunleavy and P. B. Katehi, "A generalized method for analyzing shielded thin microstrip discontinuities," *IEEE Trans. Microwave Theory Tech.*, vol. 36, pp. 1758–1766, Dec. 1988.
[11] I. S. Gradshteyn and I. M. Ryzhik, *Tables of Integrals, Series, and Products*. New York: Academic, 1980.
[12] P. B. Katehi and N. G. Alexopoulous, "Frequency-dependent characteristics of microstrip discontinuities in millimeter-waves integrated circuits," *IEEE Trans. Microwave Theory Tech.*, vol. MTT-33, pp. 1029–1035, Oct. 1985.
[13] E. Erdélyi, W. Magnus, F. Oberhettinger, and F. G. Tricomi, *Higher Transcendental Functions*. New York: McGraw-Hill, 1953, vol. II, Bateman Project.
[14] I. J. Bahl and P. Bhartia, *Microstrip Antennas*. Norwood, MA: Artech House, 1980.
[15] R. K. Hoffmann, *Handbook of Microwave Integrated Circuits*. Norwood, MA: Artech House, 1987.
[16] S. Marchetti, "Simplified conducting plane sector diffraction theory and EM fields singularities at sharp edges of printed circuits," *J. Electromagn. Waves Applicat.*, vol. 11, pp. 675–688, 1997.

Sandrino Marchetti (M'91) received the Dr. and Ing. degrees (*cum laude*) in electronics with telecommunication from the University of Ancona, Italy, in 1986, and the Dr. Philosophy from the University of Bath, U.K., in 1992.

From 1987 to 1991, he was a Research Fellow at the University of Bath, U.K. From 1991 to 1994 he was Research Engineer at the Laboratory LCST-INSA of Rennes, France, where he was appointed Maitre de Conference, France, 1993. During 1994 he was a Research Engineer at the Laboratoire D'Electronique, University of Nice-Sophia Antipolis, France. Since 1995 he has been involved in settling up a Metrology Laboratory, Senigallia, Italy, while performing measurements on several physical quantities and testing of equipments for industrial processes. His research topics are solutions of Maxwell equations in new coordinate systems, space-domain formulations of Green's functions for stratified media, solution of frequency- and space-domain integral equations applied to the analysis of edge effects, diffractions, and radiation in microwave and millimeter-wave integrated circuits and antennas.